

Roughness-induced critical phenomenon analogy for turbulent friction factor explained by a co-spectral budget model

Shuolin Li* and Gabriel Katul†

Department of Civil and Environmental Engineering

and Nicholas School of the Environment,

Duke University, Durham, NC, USA

Abstract

Drawing on an analogy to critical phenomena, it was shown that the Nikuradse turbulent friction factor (f_t) measurements in pipes of radius R and wall roughness r can be collapsed onto a one-dimensional curve expressed as a conveyance law $f_t Re^{1/4} = g_o(\chi)$, where Re is a bulk Reynolds number, $\chi = Re^{3/4}(r/R)$. The implicit function $g_o(\cdot)$ was conjectured based on matching two asymptotic limits of f_t . However, the connection between $g_o(\cdot)$ and the phenomenon it proclaims to represent - turbulent eddies - remains lacking. Using models for the wall-normal velocity spectrum and return-to-isotropy for pressure-strain effects to close a co-spectral density budget, a derivation of $g_o(\cdot)$ is offered. The proposed method explicitly derives the solution of the conveyance law and provides a physical interpretation of χ as a dimensionless length scale reflecting the competition between viscous sublayer thickness and characteristic height of roughness elements. The application of the proposed method to other published measurements spanning roughness and Reynolds numbers beyond the original Nikuradse range is further discussed.

* shuolin.li@duke.edu

† gaby@duke.edu

I. INTRODUCTION

A recent analogy between critical phenomena and turbulent flows was proposed to describe the turbulent friction factor f_t in pipes [15]. The f_t is a dimensionless measure of the total frictional loss defined as

$$f_t = \frac{gRS_b}{\frac{1}{2}U_b^2}, \quad (1)$$

and is presumed to vary with the bulk Reynolds number ($Re = U_b 2R/\nu$) and relative roughness of the wall (r/R), where g is the gravitational acceleration, U_b is the bulk or time and area-averaged velocity, r is a measure of the wall roughness often related to the statistics of the protrusions from the pipe wall, R is the pipe radius, ν is kinetic viscosity, and S_b is the friction slope that can be related to the driving force - the mean pressure gradient [6]. Using measured f_t , the weighty experiments by Nikuradse [32] on regular roughness elements identified two limiting flow regimes - hydrodynamically smooth and fully-rough based on competing mechanisms between r/R and a length scale measuring the thickness of the viscous sublayer $L_v = 5\eta$, where η is the Kolmogorov micro-scale. In the hydrodynamically smooth case (i.e. $r/L_v \ll 1$), $f_t = A_b Re^{-1/4}$ where $A_b = 0.316$ (labelled as the Blasius scaling) whereas in the fully-rough regime ($r/L_v \gg 1$), $f_t = A_s (r/R)^{1/3}$ where $A_s = 0.14$ (labelled as the Strickler scaling). Exploiting an analogy developed to infer thermodynamic properties of ferromagnets near critical temperatures, the Nikuradse's f_t data was shown to collapse (albeit imperfectly) onto a single curve labeled here as NG06 [15]. In the derivation of NG06, two limiting regimes occurring for $r/R \rightarrow 0$ (analogous to an external magnetic field control) and $Re^{-1} \rightarrow 0$ (analogous to inverse temperature near its critical state), respectively, have been exploited. The NG06 f_t was shown to be mathematically described by [15]

$$f_t = Re^{-1/4} g(\chi), \quad \text{with } g_o(\chi) = \begin{cases} \text{const.}, & \chi \rightarrow 0 \\ \chi^{1/3}, & \chi \rightarrow \infty \end{cases}, \quad (2)$$

where $\chi = Re^{3/4} (r/R)$ and $g_o(\cdot)$ is an implicit function satisfying two asymptotic properties: when $\chi \rightarrow 0$, equation 2 yields $f_t \sim Re^{-1/4}$ (the Blasius scaling) whereas at sufficiently large Re , $g_o(\chi)$ becomes $Re^{1/4} (r/R)^{1/3}$ resulting in $f_t \sim (r/R)^{1/3}$ (the Strickler scaling). The outcome of equation 2 is a monotonic curve along which all the Nikuradse data collapse as shown in Figure 1

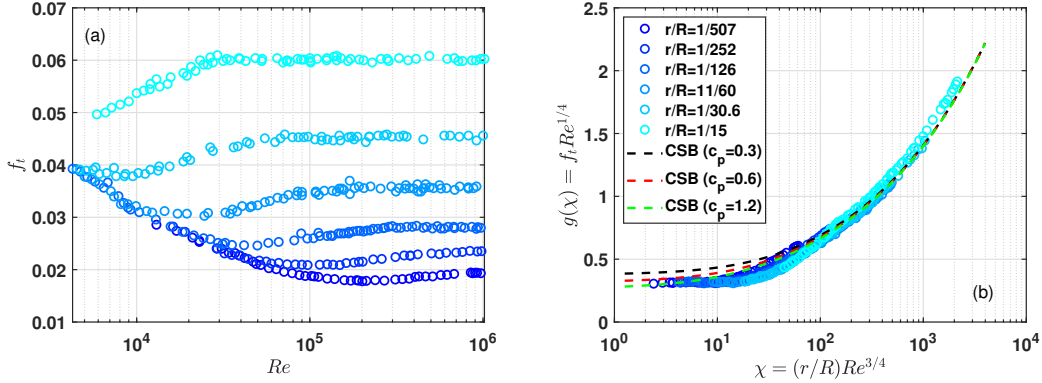


FIG. 1. The original Nikuradse diagram and its NG06 representation with $f_t Re^{1/4}$ expressed as an unknown function of χ . The coefficient $c_p = 0.61$ can be theoretically determined when combining Blasius and Strickler scaling [12].

The collapse of all Nikuradse data when representing $f_t Re^{1/4}$ as a function of χ may indicate the existence of a critical phenomenon in the turbulent friction factor [15]. The NG06 stimulated other theories and a combination of variables derived from hydrodynamic stability analysis for laminar flow [26, 40]. Other approaches to deriving f_t and refinements to NG06 exploited the so-called spectral link in turbulent flows [1, 5, 12, 13, 16, 17, 31] summarized by

$$f_t \propto \sqrt{\int_{1/l_o}^{\infty} E_{TKE}(k) dk}, \quad (3)$$

where k is wavenumber or inverse eddy size, $l_o = r + L_v$, and $E_{TKE}(k)$ is the spectrum of the turbulent kinetic energy (TKE). This relation was tested using two-dimensional soap film experiments where $E_{TKE}(k)$ was manipulated to scale as $k^{-5/3}$ or k^{-3} depending on whether the inverse energy cascade or forward enstrophy (or integral of vorticity) cascade applies [17, 25, 41]. Another corollary improvement to NG06 routed in equation 3 was intermittency corrections to phenomenological models for $E_{TKE}(k)$ [31]. When such intermittency corrections are accounted for in $E_{TKE}(k)$, a revised NG06 that better describes the otherwise imperfect fit was reported. The collapse of the Nikuradse data onto a single (albeit in a restricted range of $r/R - Re$) curve is appealing because it offers a diagnostic description of the so-called transitional regime between smooth and fully rough cases [12] or other similarity variants on it [26]. That transitional flow regimes in f_t exhibit rich scaling laws are now opening up new vistas to other analogies in physics and statistical mechan-

ics [16] though no contact with Navier-Stokes turbulence or approximations to it has been offered to date.

This work explains $g_o(\chi)$ and derives its generalization for steady and axially uniform turbulent pipe flow using standard turbulent theories. The theoretical tactic employs a co-spectral budget (CSB) model that makes contact with an approximated Navier-Stokes equation for the near-wall turbulent stress in spectral space [3, 9, 23, 24]. The outcome is an analytical formulation linking an externally specified wall-normal energy spectrum to the turbulent stress (via the CSB model), and upon scale-wise integration yields an expression for f_t analogous in form to equation 3. This expression includes a bridge between local variables formulated on a plane positioned at a wall distance z_* that scales with l_o and bulk flow variables reflecting the overall geometry and flow rate in the pipe [3, 9]. The proposed model is shown to collapse the expanded f_t data onto a single curve whose shape is explicitly derived from the CSB model with similarity constants all linked to standard constants in turbulence theories. Other mechanisms not explicitly treated such as intermittency corrections [31] (or other similarity variants [26]), to the wall-normal velocity spectrum, non-local spectral transfer across scales in energy and stresses, non-linear return-to-isotropy representations for pressure-velocity interactions, or bottle-necks in the energy cascade can all be accommodated in this framework and their effects tracked onto an NG06 type curve but they are not explicitly considered here.

II. THEORY

A. Definitions

The flow is assumed to be stationary and longitudinally homogeneous driven by a constant mean pressure-gradient within a pipe of radius R and cross-sectional area A_p . The pipe wall is uniformly covered with regular roughness elements having a protrusion amplitude r similar to the Nikuradse experiments (see Figure 2a). Defining $z = R - y$ as the normal distance to the pipe boundary, y as the distance from the pipe center, $U^+ = U(z)/u_*$ as the dimensionless mean velocity profile, $u_* = \sqrt{\tau_o/\rho_f}$ as the friction velocity, τ_o as the wall stress, ρ_f as the fluid density, the bulk (i.e. time and cross-sectional area-averaged) velocity

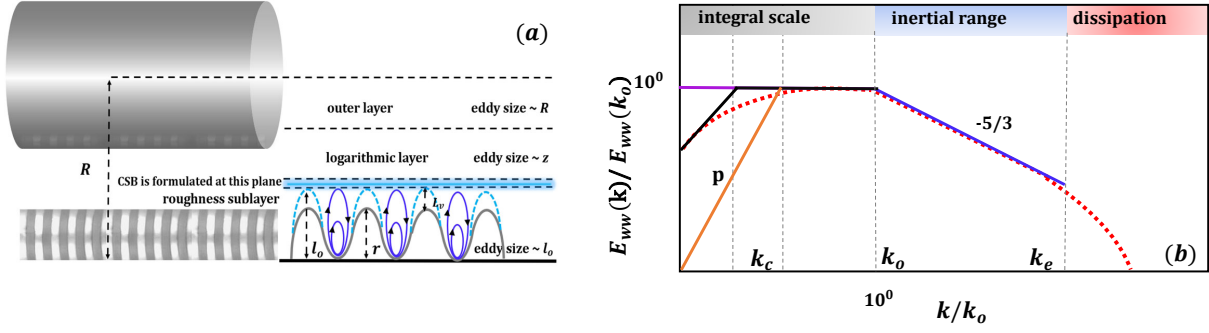


FIG. 2. (a): The formulation of the CSB model at $z_*/l_o > 1$ but below the log-region. (b): Schematic of the wall-normal velocity spectrum $E_{ww}(k)$ of a turbulent rough pipe as a function of wavenumber k . The dashed red line represents commonly observed $E_{ww}(k)$ that can be partitioned into three subranges: an energetic range (integral scale), inertial range, and viscous dissipation range. The solid lines show different models for this spectrum. Plausibility check of the assumed $E_{ww}(k)$ shape can be made using integral constrain shown in Supplementary Material.

can be determined as

$$U_b = \frac{1}{A_p} \int_0^R U(y) dA_s, \quad (4)$$

where $dA_s = 2\pi y dy$. For this setup, the mean longitudinal momentum balance reduces to a balance between the mean pressure gradient and the stress gradient given by

$$\frac{\partial P}{\partial x} = \frac{1}{y} \frac{\partial(y\tau)}{\partial y}, \quad (5)$$

where P is the mean pressure, x is the longitudinal distance along the pipe length, and $\tau(y)$ is the total shear stress at radial distance y from the pipe center. Integrating with respect to y yields

$$\tau(y) = \left(\frac{\partial P}{\partial x} \right) \frac{y}{2} + C_1, \quad (6)$$

where C_1 is determined so that at $y = 0$ (i.e. center of the pipe), $\tau(0) = 0$ due to symmetry thereby resulting in

$$\tau(y) = \left(\frac{\partial P}{\partial x} \right) \frac{y}{2}. \quad (7)$$

Defining

$$u_*^2 = \frac{\tau_o}{\rho_f} = \frac{1}{\rho_f} \frac{R}{2} \left(\frac{\partial P}{\partial x} \right) = \frac{R}{4} g S_b, \quad (8)$$

and decomposing $\tau(y)$ into a turbulent τ_t and a viscous τ_m contribution leads to the variation in total stress with distance from the wall as

$$\tau(z) = \tau_t + \tau_m = \tau_o \left(1 - \frac{z}{R}\right), \quad (9)$$

where $\tau_m = \rho_f \nu \Gamma(z)$ and $\Gamma(z) = dU/dz$.

B. The co-spectral budget model

The CSB model is now formulated at a wall-normal distance $z = z_*$ below the region where the onset of a logarithmic mean velocity profile for $U^+ = U(z)/u_*$ is expected (Figure 2). Hence, the effective eddy size l_o impacting momentum exchange at z_* need not scale with z [3, 23] but with r or L_v ($= 5\eta/2$) depending on whether the flow is rough or smooth. To accommodate rough and smooth pipe flow conditions, we define $l_o = r + L_v$ as before [9, 13], where $\eta = (\nu^3/\epsilon)^{1/4}$, and ϵ is a local turbulent kinetic energy dissipation rate evaluated at z_* . A justification for summing r and L_v is that resistances to momentum exchanges between a moving fluid and a stationary wall in the combined layer are additive, and resistances scale linearly with layer thicknesses. The following constraints on the choice of z_* are now enforced: $z_*/l_o \geq 1$ and $\tau_t(z_*)/\tau_o \approx 1$, where $\tau_t(z_*)$ is the turbulent stress at z_* labelled hereafter as τ_* for notation convenience. Selecting z_* to be sufficiently distant from the boundary also minimizes wall-blocking effects impacting U^+ in the buffer region [29]. For a rough pipe, the z_* is still expected to be in the roughness sublayer (RSL) whereas in a turbulent smooth pipe, z_* is in the upper-region of the buffer layer [34–37].

The CSB model links τ_* to eddy sizes at z_* using $\tau_*/\rho_f = -\overline{u'w'} = \int_0^\infty F_{uw}(k)dk$, and $F_{uw}(k)$ defines the co-spectrum between u' and w' at k (or inverse eddy-size), u' and w' are the turbulent longitudinal and wall-normal velocity components, respectively, primed quantities are excursions from the mean state, and overline is averaging over coordinates of statistical homogeneity (usually surrogated to time averaging). The terms governing the time evolution of the co-spectral budget at z_* are [23, 24]

$$\frac{\partial F_{uw}(k)}{\partial t} = P_{uw}(k) + T_{uw}(k) + [\pi_{uw}(k) - D_{uw}(k)], \quad (10)$$

where $P_{uw}(k) = \Gamma(z)E_{ww}(k)$ is the turbulent stress production term at wavenumber k due to the presence of a mean velocity gradient Γ , $E_{ww}(k)$ is the energy spectrum of the

wall-normal velocity component, $T_{uw}(k)$ is a scale-wise transfer of momentum and satisfies $\int_0^\infty T_{uw}(k)dk = 0$, $\pi_{uw}(k)$ is a pressure-velocity de-correlation term commonly modeled using return to isotropy principles, and $D_{uw}(k) = 2\nu k^2 F_{uw}(k)$ is a viscous dissipation term also responsible for de-correlating u' from w' . Stationarity is assumed through out and closure models for $\pi_{uw}(k)$ and $T_{uw}(k)$ are needed. For maximum simplicity and to ensure a recovery of $F_{uw}(k) \propto k^{-7/3}$ in the so-called inertial subrange (ISR), $T_{uw}(k) = 0$ is assumed (and justified later on). Adopting a linear Rotta scheme revised for isotropization of the production at any k , $\pi_{uw}(k)$ is closed by [3, 9, 23, 24, 29]

$$\pi_{uw}(k) = -C_R \frac{1}{t_r(k)} F_{uw}(k) - C_I P_{uw}(k), \quad (11)$$

where $C_R \approx 1.8$ and $C_I = 3/5$ [35] are the Rotta and isotropization of production constants, and $t_r(k) = [k^3 E_{kol}(k)]^{-1/2}$ is a local wavenumber dependent relaxation time scale [33, 35] based on a Kolmogorov spectrum $E_{kol}(k)$. Other possibilities that include non-local energy transfer can be accommodated using $t_r(k)$. For example, a non-local closure for the energy flux is the Heisenberg model [18] that can be re-casted as $t_r(k)^{-1} = \sqrt{\int_0^k p^2 E_{kol}(p) dp}$ [21]. There are issues with the Heisenberg model related to the directional energy transfer and equipartition of energy that have already been identified and discussed [7]. For this reason, the focus here is maintained on the simpler $t_r(k) = [k^3 E_{kol}(k)]^{-1/2}$. The $t_r(k)$ becomes unbounded as $k \rightarrow 0$ necessitating additional constraints at large scales. One possible constraint is to set $t_r(k) = t_r(k_c)$ when $k/k_c < 1$ where $k_c = 1/R$ is the smallest inverse length scale over which $E_{uw}(k)$ energy transfer occurs downscale. The two destruction terms in the CSB model, the Rotta component of $\pi_{uw}(k)$ and viscous destruction $D_{uw}(k)$, are compared at small scales (or large k) using

$$\Phi(k) = \frac{2\nu k^2 F_{uw}(k)}{C_R F_{uw}(k)/t_r(k)} = \frac{2}{C_R} (k\eta)^{4/3}, \quad (12)$$

where the role of $P_{uw}(k)$ has been ignored at large k for simplicity. When $k\eta \ll 1$, the viscous dissipation is negligible ($\Phi(k) \approx 0$) compared with the Rotta term. However, as $k\eta > 1$, the viscous term dominates and $\Phi^{-1}(k) \approx 0$. Adopting the aforementioned closure schemes, the co-spectrum at k is derived as

$$F_{uw}(k) = \frac{1 - C_I}{C_R} \Gamma(z_*) \frac{E_{uw}(k) t_r(k)}{\Phi(k) + 1}. \quad (13)$$

The co-spectrum must be integrated across all k to yield τ_* needed in the determination of f_t . To evaluate $F_{uw}(k)$, the shape of $E_{uw}(k)$ is required and discussed in Figure 2.

The $E_{ww}(k)$ in the ISR is given by the Kolmogorov spectrum $E_{kol}(k) = C_o [\epsilon(z_*)]^{2/3} k^{-5/3}$ where $C_o = (24/55)C'_o$ is the Kolmogorov constant for the wall-normal velocity component [35] related to the Kolmogorov constant for the turbulent kinetic energy spectrum ($C'_o = 1.5$). Deviations from E_{kol} at other scales are specified as follows: i) an exponential cutoff, $f_\eta = \exp\left[-\beta\left(\frac{1}{2}C_R\Phi\right)^{3/4}\right] \approx 1$, when $k \ll k_e$, where $\beta = 2.1$, to resolve the viscous dissipation range [14, 35]; ii) two piece-wise functions for the energetic range [3]. The $E_{ww}(k)$ is

$$E_{ww}(k) = \begin{cases} E_{kol}(k_o)k_c^{-p}k^p & \text{if } 0 \leq k \leq k_c \\ E_{kol}(k_o) & \text{if } k_c \leq k \leq k_o \\ E_{kol}(k)f_\eta & \text{otherwise} \end{cases} \quad (14)$$

where $k_c = 1/R$, $k_o = 1/l_o$, $k_e = 1/\eta$ are three characteristic wavenumbers that mark the key transitions in $E_{ww}(k)$ as related to pipe radius, characteristic eddy scale in the RSL, and the viscous length scale [3, 9, 24, 27, 35], and several theories constrain p to be between 2 (Saffman spectrum) and 4 (Batchelor spectrum). The p remains uncertain though various turbulence theories suggest a numerical value of $p = 2$ (Saffman spectrum), $p = 8/3$ (von Kármán spectrum) or $p = 4$ (Batchelor spectrum) reviewed elsewhere [35]. All theories agree that $p > 1$ to ensure that as $k \rightarrow 0$, both $E_{ww}(k) \rightarrow 0$ and $(dE_{ww}(k)/dk) \sim k^{p-1} \rightarrow 0$. Notwithstanding this uncertainty in p , its precise numerical value does not alter the scale-wise integrated outcome. A plausibility check on the assumed shape of $E_{ww}(k)$ is conducted using the integral constraint $\sigma_w^2 = \int_0^\infty E_{ww}(k)dk$, yielding

$$\sigma_w^2 \approx \left[1.63 - \frac{0.65p}{p+1} \left(\frac{l_o}{R}\right) - 0.69 \left(\frac{\eta}{l_o}\right)^{2/3} \right] u_*^2, \quad (15)$$

where a balance between production and dissipation of TKE yields $\epsilon(z_*) \approx u_*^2\Gamma(z_*)$ and $\Gamma(z_*) = u_*/l_o$. Equation 15 predicts a maximum $\sigma_w/u_* = \sqrt{1.63} = 1.28$ sufficiently close to the reported 1.1 – 1.25 range in near-neutral atmospheric flows, open channels, and pipes [9, 20, 34, 36, 37].

Equation 13 can be further analyzed for the much-studied ISR and is shown to be consistent in both scaling law and similarity coefficients with accepted theories and experiments [35, 38]. For example, in the ISR, $\Phi(k) \ll 1$, and the co-spectrum reduces to

$$F_{ww}(k) = \sqrt{C_o} \frac{(1 - C_I)}{C_R} \Gamma(z_*) [\epsilon(z_*)]^{1/3} k^{-7/3}, \quad (16)$$

consistent with well-accepted co-spectral theories predicting $k^{-7/3}$ scaling [28, 35]. The emerging constants $\sqrt{C_o}(1 - C_I)/C_R = 0.18$ is also close to the accepted similarity constant

reported in laboratory and field experiments as well as direct numerical simulations (0.15) discussed elsewhere [4, 24, 38, 42]. These findings indirectly support setting $T_{uw}(k) = 0$ for all k as a first-order approximation in two ways: (i) its expected zero value in the ISR is needed to recover the $k^{-7/3}$ scaling, and (ii) $T_{uw}(k)$ must satisfy the integral constraint $\int_0^\infty T_{uw}(k)dk = 0$ by definition. In the case of $E_{kol}(k)$, the transfer of energy across scales shapes the energy cascade and is thus necessary for obtaining the $k^{-5/3}$ scaling in the ISR. The inclusion of the transfer term in the energy cascade (indirectly specified by $E_{uw}(k)$) but not in the CSB may appear paradoxical. This is not so as the role and significance of the transfer terms are quite different when analyzing scale-wise energy and scale-wise stress budgets [4]. Last, when $\Gamma(z) = 0$, $F_{uw}(k) = 0$ at all k . Hence, a finite $\Gamma(z_*)$ is necessary to maintain a finite co-spectrum at all k and $f_t > 0$.

Returning to the determination of f_t , upon inserting equation 14 into 13 yields the near-bed shear stress in terms of $f_t (= 8\tau_*/\rho_f U_b^2)$ as

$$\begin{aligned} \frac{f_t U_b^2}{8} = \frac{\xi(z_*)}{A_\pi} & \left[\int_0^{k_c} k_c^{-p-2/3} k_o^{-5/3} k^p dk + \int_{k_c}^{k_o} k_o^{-5/3} k^{-2/3} dk \right. \\ & \left. + \int_{k_o}^{k_e} k^{-7/3} dk + B_\pi \int_{k_e}^{+\infty} k_e^{4/3} k^{-11/3} \exp(-\beta k \eta) dk \right], \end{aligned} \quad (17)$$

where $A_\pi = C_R/[\sqrt{C_o}(1 - C_I)] \approx 5.58$, $B_\pi = (5^{4/3}/2) C_R \sqrt{C_o} \approx 6.20$, and $\xi(z_*) = \Gamma(z_*)[\epsilon(z_*)]^{1/3}$. The four integrand functions are contributions to the turbulent stress arising from the two energetic, inertial, and dissipation ranges, respectively.

III. RESULTS

A. Linking local and bulk variables

The terms $\Gamma(z_*)$ and $\epsilon(z_*)$ needed in $\xi(z_*)$ are defined at z_* and must be linked to bulk variables to complete the CSB model for f_t . These are commonly estimated as [3, 9]

$$\Gamma(z_*) = \frac{u_*}{l_o} = c_t \frac{U_b - 0}{l_o}, \quad \epsilon(z_*) = \frac{u_*^3}{l_o} = c_p^3 \frac{U_b^3}{R}, \quad (18)$$

where $c_t(z_*)$ and $c_p(z_*)$ are unknown positive coefficients that link local to bulk variables given by $c_t = u_*/U_b$ and $c_p = (u_*/U_b)(R/l_o)^{1/3} = c_t(R/l_o)^{1/3}$. A bulk dissipation proportional to U_b^3/R is compatible with upper limits set by prior variational analysis [10]. Clearly, c_t and c_p cannot be individually constant and must vary with f_t [3, 9]. The interest here

is not in their individual variations but in their product. Increasing l_o increases c_p (more dissipation for the same U_b or flow rate) but decreases c_t because U_b overestimates $U(z_*)$ thus making their product less sensitive to l_o as shown elsewhere [3, 9].

For guessing a $c_t c_p$, several possibilities exist including the use of complete and incomplete similarity or covariate analysis [2]. Another naive possibility is to assume $c_t c_p$ varies with the primary variable R/l_o and proceed to select a maximum $c_t c_p$ at a given R/l_o . By definition, $c_t c_p \sim (u_*/U_b)^2 (R/l_o)^{1/3}$. With $s = R/l_o$, assuming $G_f(s) = (u_*/U_b)^2$ and maximizing $c_t c_p$ at a given s leads to

$$\frac{d}{ds}(c_t c_p) = \left[\frac{G_f(s)}{3s^{2/3}} + s^{1/3} \frac{d}{ds} G_f(s) \right] = 0. \quad (19)$$

The solution of equation 19 is $G_f(s) = b_o s^{-1/3}$, where b_o is a constant independent of $s = R/l_o$. This argument is congruent with complete similarity theory in the limit of very large R/l_o but cannot be correct for all R/l_o . Accepting momentarily a constant $c_t c_p$ at its maximal value, f_t can be linked to r/R and Re at any finite R/l_o using

$$f_t = \frac{30(c_t c_p)}{A_\pi} \left[-Y(p) \left(\frac{k_c}{k_o} \right)^{2/3} + \left(\frac{k_c}{k_o} \right)^{1/3} - C_\pi \left(\frac{k_c}{k_e} \right)^{1/3} \frac{k_o}{k_e} \right], \quad (20)$$

where

$$Y(p) = \frac{12p + 8}{15(p + 1)}, \quad C_\pi = \frac{1}{5} - \frac{4\sqrt[3]{5}}{1875} \beta^{\frac{8}{3}} \Gamma_{o,*} \left(-\frac{8}{3}, \frac{\beta}{5} \right),$$

$\Gamma_{o,*}(\cdot)$ is the Gamma function and $C_\pi \approx 0.146$. For $p = 2 - 4$, $Y(p) \approx 0.72 - 0.75$ and variations in p are hereafter ignored. The two extreme cases, Strickler and Blasius scaling are now evaluated. In a rough pipe where $r/L_v \gg 1$, $DS(k)$ can be ignored and $k_e = k_o(r/\eta) \rightarrow \infty$ allowing the IR to extend to $k_e \rightarrow \infty$. In the limit of $r/R \ll 1$, the leading order term in equation 20 is

$$f_t \approx \frac{30}{A_\pi} c_p c_t \left(\frac{r}{R} \right)^{1/3}. \quad (21)$$

Hence, the Strickler scaling requires: i) a constant $c_p c_t (= A_s A_\pi / 30 \approx 0.026$ to recover the Nikuradse data), ii) $r/L_v \gg 1$, and iii) $r/R \ll 1$. Likewise, when $r/L_v \ll 1$ so that $l_o \approx L_v$, the inertial subrange commences at k_e and rapidly terminates into a dissipation range since $k_r/k_e \ll 1$. The viscous cutoff effects become important when $k > k_e$ revising equation 20 to

$$f_t \approx \frac{30 D_\pi}{A_\pi} c_t c_p \left(\frac{\eta}{R} \right)^{1/3} = \frac{30 D_\pi}{2^{-1/4} A_\pi} c_t c_p^{3/4} Re^{-1/4}, \quad (22)$$

where $D_\pi = \sqrt[3]{5} - C_\pi/5 \approx 1.68$, $(R/\eta)^{1/3} = (c_p Re/2)^{1/4}$. The Blasius scaling requires $c_t c_p^{3/4} (= 2^{-1/4} A_b A_\pi / (30 D_\pi) \approx 0.0294$ for Nikuradse data) not to vary with Re (or equivalently

$c_t c_p$ not to vary with R/l_o when $l_o = L_v$ as before). Equation 20 allows separating the effects of turbulent exchanges of momentum at z_* from relations between local (at z_*) and bulk variables (encoded in $c_t c_p$) when evaluating f_t or NG06.

B. Solution of the implicit function in NG06

The study objective, which is to derive the $g_o(\chi)$ in NG06 for the Nikuradse data ($r/R \ll 1$) and regular roughness, can now be addressed. The $g_o(\chi)$ can be made explicit when rearranging equation 20 to yield,

$$g_o(\chi) = (c_t c_p^{3/4}) \frac{30}{2^{-1/4} A_\pi} \left\{ \left[\left(\frac{c_p}{2} \right)^{3/4} \chi + 5 \right]^{1/3} - C_\pi \left[\left(\frac{c_p}{2} \right)^{3/4} \chi + 5 \right]^{-1} \right\}, \quad (23)$$

where $\chi = Re^{3/4}(r/R)$ derived from $\chi = (2/c_p)^{3/4}(r/\eta)$. Now equation 23 explains why the Nikuradse data imperfectly collapses along a unique curve when plotting $f_t Re^{1/4}$ versus $Re^{3/4}(r/R)$ under the restrictive assumption of constant $c_t c_p$. Thus, the main novelty here is to show that the $g_o(\chi)$ in NG06 can be linked to an approximated Navier-Stokes equation (i.e. the CSB model) provided $c_t c_p$ is constant at maximal value, which is the sought result. The solution of equation 23 is also presented in Figure 1 where $c_p = 2(D_\pi A_s/A_b)^4 \approx 0.6$ and can be directly derived when combining the Strickler and Blasius scaling laws. Moreover, a sensitivity analysis was conducted by setting $c_p = 0.3, 1.2$ to find the best fit between equation 23 and the Nikuradse data set. Figure 1 shows that setting c_p as constant (accepting Blasius and Strickler scaling laws simultaneously) can indeed replicate the NG06 result to a leading order, but further investigations are needed when $\chi < 20$.

IV. DISCUSSION

A. Extension to micro-scale and large-scale roughness

Moving beyond the widely-used Nikuradse data range for $r/R < 0.1$ and for regular roughness elements, the following discussion are presented to assess the plausibility of extending the implicit function $g_o(\chi)$ to two extreme cases as shown in Figure 4: i) a hydrodynamically smooth regime or the micro-scale roughness $r/R \in [10^{-6}, 10^{-5}]$ from Hi-Reff [11] super-pipe experiments (the Oregon and Princeton [30, 39] are assumed smooth though no r/R measurements were reported), and (ii) a large-scale roughness regime $r/R \in [0.1, 0.2]$ from pipes

roughened with single layers of sand [19]. The reported friction factor data [19] (runs $R4$ and $R5$) in the original Table 1 were employed. These two runs can still be approximated as regular roughness with r/R not too large so that the prior conditions imposed on z_* for the use of the CSB can still be enforced.

B. Estimation of $c_t c_p$

To extend the proposed model and without invoking further *ad hoc* assumptions on the local flow structure, a 'naive' but direct approach is to revise the constant c_t , c_p assumption that seems only applicable to the Nikuradse range [9, 12]. When inferring U_b , the log-law is assumed to populate U^+ over extensive portions of the pipe area at intermediate to high Re . The log-law overestimates U^+ in the buffer region (for smooth pipes) or the roughness sublayer (in rough pipes) but underestimates U^+ in the wake-region [23]. Thus, its area-integrated form from l_o to R may be less sensitive to such deviations and provides a leading order guess as to whether $c_t c_p$ is constant or variable. With this idealized U^+ representation, it follows that $c_t^{-1} \approx U_b/u_* = (1/\kappa) \ln(R/l_o) + B_o$, where B_o is an integration constant of order unity and κ is the von Kármán constant [35]. For this c_t and $c_p = c_t(R/l_o)^{1/3}$, their product can now be estimated as

$$c_t c_p \approx \left(\frac{R}{l_o}\right)^{1/3} \left[\frac{1}{\kappa} \ln\left(\frac{R}{l_o}\right) + B_o \right]^{-2}, \quad (24)$$

Increasing R/l_o increases both numerator and denominator thereby making their ratio less sensitive to R/l_o as expected. However, a near constant $c_t c_p$ emerges when noting that for large but finite R/l_o , $\ln(R/l_o) \approx A_n(R/l_o)^{n_o}$ with $n_o = 1/6$ for the range covered by R/l_o in many experiments [22]. To elaborate, the limiting case for large R/l_o is considered and this case leads to

$$n_o \approx \lim_{R/l_o \rightarrow \infty} \frac{\log[\log(R/l_o)]}{\log(A_n) + \log(R/l_o)} \approx \frac{1}{\log(R/l_o)} \quad (25)$$

when applying L'Hôpital's rule. The $n_o = 1/\log(R/l_o)$ appears independent of A_n but weakly depends on R/l_o as shown from a similar argument using asymptotic covariance analysis [2]. In general, $n_o \rightarrow 1/\log(R/l_o)$ for very large R/l_o and cannot be a constant. To explore the plausibility of setting $c_t c_p$ a constant beyond the Nikuradse experiments, other predictions from the virtual Nikuradse [43] equation (VN), the Moody diagram summarized

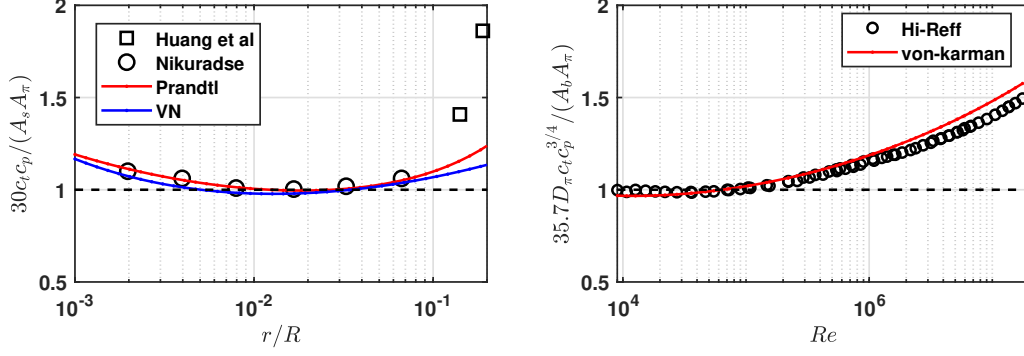


FIG. 3. Exploring the similarity coefficient of Strickler and Blasius scalings. The data sets are normalized by A_s and A_b , the similarity coefficients for the Strickler and Blasius formulae, respectively where the purple line highlights the unit line. Other than the experimental data, the blue lines represents the predictions from Prandtl and von Kármán equations (or the Colebrook-White formula when added), and the black dashed line features the prediction from virtual Nikuradse curves.

by the approximate von Kármán equation [8]), and the aforementioned micro-scale and large-scale roughness data are employed and discussed in Figure 3.

Figure 3 shows that $c_t c_p$ does not vary appreciably with r/R for small-scale roughness ($r/R < 0.1$) consistent with the range of applicability [3, 9]. However, as r/R increases to 0.2, $c_t c_p$ increases leading to a break-down in the Strickler scaling. This breakdown originates from estimates of $\xi(z_*)$ when using bulk variables and not in the particulars of momentum exchange by turbulent eddies at z_* represented by the CSB model. Likewise, for the Blasius scaling the $c_t c_p^{3/4}$ (or $c_t c_p$ independent of R/L_v) remains flat for a restricted range of $Re \in [10^4, 10^5]$ but increases significantly with increasing Re .

With modeled $c_t c_p$ provided in equation 24, a representation of extended Nikuradese diagram with additional micro-scale and large-scale roughness data is shown in Figure 4. Figure 4 shows that all these f_t data reasonably collapse along a one-dimensional curve (predicted from CSB) when plotted versus l_o/R . This finding indicates that l_o/R is a characteristic length scale that describes f_t in all regimes as alluded to in earlier studies [3, 9]. Similar to the data collapse strategy that NG06 employed, an apparent curve can also be derived when plotting $f_t \cdot (l_o/R)$ versus l_o/R , where $f_t \cdot (l_o/R)$ can be understood physically as a 'roughness friction factor' noting that $f_t(l_o/R) = 2gl_o S_b / U_b^2$. The improved data collapse

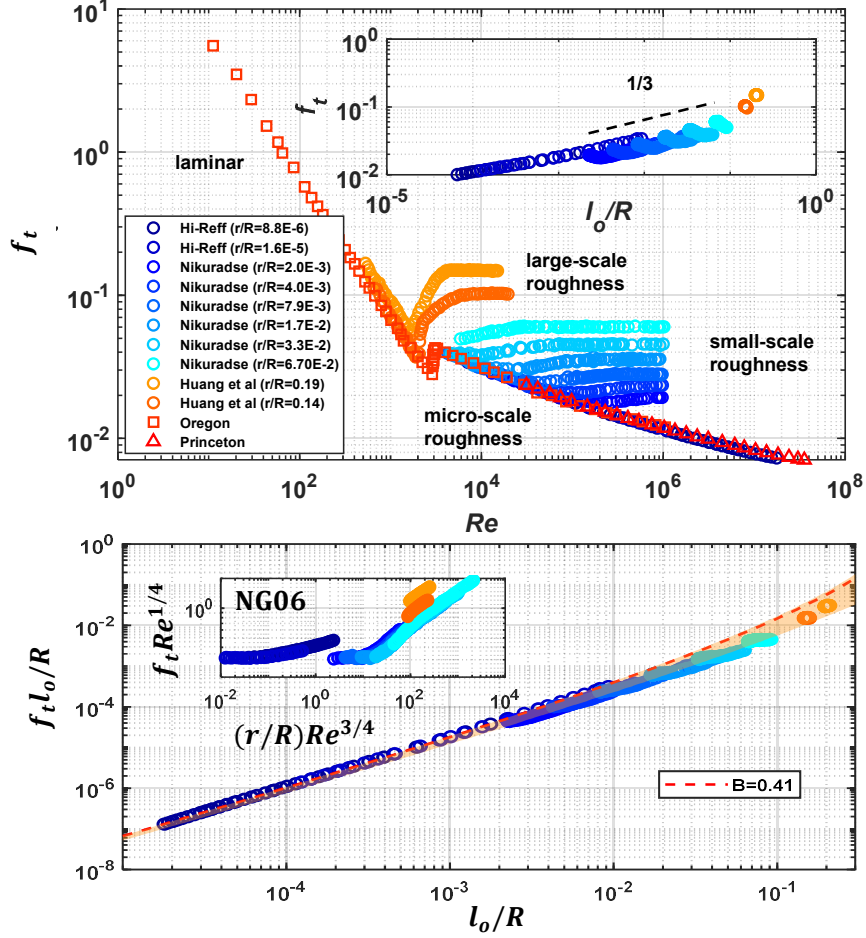


FIG. 4. Representation f_t across regular roughness elements. The top panel shows the expanded Nikuradse diagram using wider experimental conditions, including the large-scale roughness [19], intermediate/small-scale roughness [32], and smooth-wall [11, 30, 39]. The inset is a representation of all f_t data with l_o/R as a general scale using the turbulence data (excluding non-turbulent regimes). The bottom panel shows the data collapse of $f_t(l_o/R)$ versus l_o/R where the orange band features CSB prediction with $B_o \in [0.04, 4]$. The inset is the NG06 curve for the same data.

from the $f_t \cdot (l_o/R)$ representation is partly connected to self-correlation because the abscissa and ordinate now share the same variable (l_o/R) that span several orders of magnitude. Likewise, the NG06 representation also suffers from similar self-correlation through Re , which varies over several orders of magnitude as well. This finding confirms the applicability of the proposed CSB model at the two extremes of (l_o/R) albeit models for $c_t c_p$ are required as deviations from a constant product value are expected. These deviations are connected to how bulk variables relate to local mean velocity gradient and TKE dissipation rate at z_*

instead of how eddies transport momentum to pipe walls at z_* .

V. CONCLUSION

An explicit solution for the NG06 conveyance equation for friction factor, originally conjectured from analogies to critical phenomenon, was derived from a CSB model. The CSB model employs standard turbulent theories and a commonly accepted wall-normal velocity spectrum. The model closes the pressure-velocity de-correlation term using a linear Rotta scheme based on linear return-to-isotropy with adjustments due to isotropization of the production term. Moving beyond and above the CSB model, the extension of the CSB prediction is also discussed in terms of micro-scale roughness and large-scale roughness experiments that were not covered by the original Nikuradse range. The analysis shows that all the turbulent friction factor data collected so far can be approximately collapsed onto a single curve. However, the work here shows that much of the uncertainty originates from how local to bulk variables are related instead of the mechanics of momentum exchange with the pipe walls.

Acknowledgements: Support from the U.S. National Science Foundation (NSF-AGS-1644382, NSF-AGS-2028633, and NSF-IOS-1754893) is acknowledged.

-
- [1] ANBARLOOEI, HR, CRUZ, DOA & RAMOS, F 2020 New power-law scaling for friction factor of extreme Reynolds number pipe flows. *Physics of Fluids* **32** (9), 095121.
 - [2] BARENBLATT, GI & GOLDENFELD, NIGEL 1995 Does fully developed turbulence exist? reynolds number independence versus asymptotic covariance. *Physics of Fluids* **7** (12), 3078–3082.
 - [3] BONETTI, S, MANOLI, GABRIELE, MANES, C, PORPORATO, A & KATUL, GG 2017 Manning’s formula and Strickler’s scaling explained by a co-spectral budget model. *Journal of Fluid Mechanics* **812**, 1189–1212.
 - [4] BOS, WJT, TOUIL, H, SHAO, L & BERTOGLIO, J-P 2004 On the behavior of the velocity-scalar cross correlation spectrum in the inertial range. *Physics of Fluids* **16** (10), 3818–3823.
 - [5] CALZETTA, E 2009 Friction factor for turbulent flow in rough pipes from Heisenberg’s closure

- hypothesis. *Physical Review E* **79** (5), 056311.
- [6] CLARK, MARK M 2011 *Transport modeling for environmental engineers and scientists*. John Wiley & Sons.
- [7] CLARK, TT, RUBINSTEIN, R & WEINSTOCK, J 2009 Reassessment of the classical turbulence closures: the Leith diffusion model. *Journal of Turbulence* (10), N35.
- [8] COLEBROOK, CYRIL FRANK, BLENCH, T, CHATLEY, H, ESSEX, EH, FINNIECOME, JR, LACEY, G, WILLIAMSON, J & MACDONALD, GG 1939 Correspondence: Turbulent flow in pipes with particular reference to the transition region between the smooth and rough pipe laws (includes plates). *Journal of the Institution of Civil engineers* **12** (8), 393–422.
- [9] COSCARELLA, FRANCESCO, GAUDIO, ROBERTO, KATUL, GABRIEL G & MANES, COSTANTINO 2021 Relation between the spectral properties of wall turbulence and the scaling of the darcy-weisbach friction factor. *Physical Review Fluids* **6** (5), 054601.
- [10] DOERING, CHARLES R & CONSTANTIN, PETER 1994 Variational bounds on energy dissipation in incompressible flows: shear flow. *Physical Review E* **49** (5), 4087.
- [11] FURUICHI, N, TERAOKA, Y, WADA, Y & TSUJI, Y 2015 Friction factor and mean velocity profile for pipe flow at high Reynolds numbers. *Physics of Fluids* **27** (9), 095108.
- [12] GIOIA, G & BOMBARDELLI, FA 2001 Scaling and similarity in rough channel flows. *Physical Review Letters* **88** (1), 014501.
- [13] GIOIA, GUSTAVO & CHAKRABORTY, PINAKI 2006 Turbulent friction in rough pipes and the energy spectrum of the phenomenological theory. *Physical Review Letters* **96** (4), 044502.
- [14] GIOIA, GUSTAVO, GUTTENBERG, NICHOLAS, GOLDENFELD, NIGEL & CHAKRABORTY, PINAKI 2010 Spectral theory of the turbulent mean-velocity profile. *Physical Review Letters* **105** (18), 184501.
- [15] GOLDENFELD, NIGEL 2006 Roughness-induced critical phenomena in a turbulent flow. *Physical Review Letters* **96** (4), 044503.
- [16] GOLDENFELD, N & SHIH, HY 2017 Turbulence as a problem in non-equilibrium statistical mechanics. *Journal of Statistical Physics* **167** (3-4), 575–594.
- [17] GUTTENBERG, N & GOLDENFELD, N 2009 Friction factor of two-dimensional rough-boundary turbulent soap film flows. *Physical Review E* **79** (6), 065306.
- [18] HEISENBERG, W 1948 On the theory of statistical and isotropic turbulence. *Proceedings of the Royal Society of London. Series A. Mathematical and Physical Sciences* **195** (1042), 402–406.

- [19] HUANG, K, WAN, JW, CHEN, CX, LI, YQ, MAO, DF & ZHANG, MY 2013 Experimental investigation on friction factor in pipes with large roughness. *Experimental Thermal and Fluid Science* **50**, 147–153.
- [20] KATUL, GG, FINKELSTEIN, PL, CLARKE, JF & ELLESTAD, TG 1996 An investigation of the conditional sampling method used to estimate fluxes of active, reactive, and passive scalars. *Journal of Applied Meteorology* **35** (10), 1835–1845.
- [21] KATUL, G., PORPORATO, A. & NIKORA, V. 2012 Existence of k^{-1} power-law scaling in the equilibrium regions of wall-bounded turbulence explained by Heisenberg’s eddy viscosity. *Physical Review E* **86** (6), 066311.
- [22] KATUL, GABRIEL, WIBERG, PATRICIA, ALBERTSON, JOHN & HORNBERGER, GEORGE 2002 A mixing layer theory for flow resistance in shallow streams. *Water Resources Research* **38** (11), 32–1.
- [23] KATUL, GABRIEL G & MANES, COSTANTINO 2014 Cospectral budget of turbulence explains the bulk properties of smooth pipe flow. *Physical Review E* **90** (6), 063008.
- [24] KATUL, GABRIEL G, PORPORATO, AMILCARE, MANES, COSTANTINO & MENEVEAU, CHARLES 2013 Co-spectrum and mean velocity in turbulent boundary layers. *Physics of Fluids* **25** (9), 091702.
- [25] KELLAY, H, TRAN, T, GOLDBURG, W, GOLDENFELD, N, GIOIA, G & CHAKRABORTY, P 2012 Testing a missing spectral link in turbulence. *Physical Review Letters* **109** (25), 254502.
- [26] LI, SHUOLIN & HUAI, WENXIN 2016 United formula for the friction factor in the turbulent region of pipe flow. *PloS One* **11** (5), e0154408.
- [27] LI, SHUOLIN & KATUL, GABRIEL 2019 Cospectral budget model describes incipient sediment motion in turbulent flows. *Physical Review Fluids* **4** (9), 093801.
- [28] LUMLEY, JL 1967 Similarity and the turbulent energy spectrum. *The Physics of Fluids* **10** (4), 855–858.
- [29] MCCOLL, KA, KATUL, GG, GENTINE, P & ENTEKHABI, D 2016 Mean-velocity profile of smooth channel flow explained by a cospectral budget model with wall-blockage. *Physics of Fluids* **28** (3), 035107.
- [30] MCKEON, BJ, SWANSON, CJ, ZAGAROLA, MV, DONNELLY, RJ & SMITS, AJ 2004 Friction factors for smooth pipe flow. *Journal of Fluid Mechanics* **511**, 41.
- [31] MEHRAFARIN, M & POURTOLAMI, N 2008 Intermittency and rough-pipe turbulence. *Physical*

- Review E* **77** (5), 055304.
- [32] NIKURADSE, JOHANN & OTHERS 1950 *Laws of flow in rough pipes*, , vol. 2. National Advisory Committee for Aeronautics Washington.
- [33] ONSAGER, L 1949 Statistical hydrodynamics. *Il Nuovo Cimento (1943-1954)* **6** (2), 279–287.
- [34] POGGI, D, PORPORATO, A & RIDOLFI, L 2002 An experimental contribution to near-wall measurements by means of a special laser Doppler anemometry technique. *Experiments in Fluids* **32** (3), 366–375.
- [35] POPE, SB 2000 *Turbulent Flows*. Cambridge University Press, Cambridge, U.K.
- [36] RAUPACH, MR 1981 Conditional statistics of Reynolds stress in rough-wall and smooth-wall turbulent boundary layers. *Journal of Fluid Mechanics* **108**, 363–382.
- [37] RAUPACH, MR, ANTONIA, RA & RAJAGOPALAN, S 1991 Rough-wall turbulent boundary layers. *Applied Mechanics Reviews* **44** (1), 1–25.
- [38] SADDUGHI, SEYED G & VEERAVALLI, SRINIVAS V 1994 Local isotropy in turbulent boundary layers at high reynolds number. *Journal of Fluid Mechanics* **268**, 333–372.
- [39] SWANSON, CHRIS J, JULIAN, BRIAN, IHAS, GARY G & DONNELLY, RUSSELL J 2002 Pipe flow measurements over a wide range of Reynolds numbers using liquid helium and various gases. *Journal of Fluid Mechanics* **461**, 51.
- [40] TAO, JIANJUN 2009 Critical instability and friction scaling of fluid flows through pipes with rough inner surfaces. *Physical Review Letters* **103** (26), 264502.
- [41] TRAN, T, CHAKRABORTY, P, GUTTENBERG, N, PRESCOTT, A, KELLAY, H, GOLDBURG, W, GOLDENFELD, N & GIOIA, G 2010 Macroscopic effects of the spectral structure in turbulent flows. *Nature Physics* **6** (6), 438.
- [42] WYNGAARD, JC & COTÉ, OR 1972 Cospectral similarity in the atmospheric surface layer. *Quarterly Journal of the Royal Meteorological Society* **98** (417), 590–603.
- [43] YANG, BOBBY H & JOSEPH, DANIEL D 2009 Virtual Nikuradse. *Journal of Turbulence* (10), N11.